Applications of satellite data in estimating heat fluxes

Olga T. Sato[1], Paulo S. Polito[1] and W. Timothy Liu[2]

Abstract. The oceanic heat budget is a balance of heat storage rate, heat flux at the air–sea interface, and horizontal divergence of oceanic heat flux. The use of satellite altimeter data makes it possible to continuously monitor the oceanic heat flux components with unprecedented resolution in both space and time. Here we present how to estimate oceanic heat storage and Ekman heat flux from a remotely sensed data perspective.
Oceanic heat storage and its time rate of change are correlated to the sea surface height anomaly signals from the TOPEX/Poseidon altimeter data. The height anomaly data are decomposed into basin-scale (seasonal), westward propagating (Rossby waves), eastward propagating (Kelvin waves), meso–scale eddies signals, and a small-scale residual. Since variability in sea surface height is mostly due to expansion and contraction of the water column it can be correlated with variations in the heat and salt content. Therefore, estimation of heat storage from altimeter data, when compared to in situ estimates, requires corrections for the haline effect. Correlations and rms differences are calculated to compare heat storage estimates based on altimeter and in situ data. The results show that heat storage anomaly can be estimated from altimeter data. For the studied regions, the haline corrections based on climatology provide equivalent or worse results than not applying a correction at all.
A large fraction of the total oceanic heat flux is associated with Ekman dynamics. The high resolution and global coverage of satellite scatterometer wind data (1992-1998) is particularly well suited to resolve the various spectral bands of temporal and spatial variability associated with Ekman layer fluxes. In agreement with previous studies, the annual zonally integrated Ekman heat flux is poleward at latitudes lower that 30° and equatorward at high latitudes. A significant part of the difference between our results and previous studies can be attributed to the choice of the definition of the temperature of the Ekman layer. The zonally averaged mean and amplitude of the annual cycle of the scatterometer based estimates are smaller compared to climatology but similar to other satellite based estimates (SSMI). The relative importance of the zonal wind stress variability components is a function of latitude. It can be divided in at least two major regimes at 15° latitude.

Introduction

The poleward heat transported by the oceans could be a good indicator for interannual or long–term climate changes. The amount of heat advected meridionally by the ocean is a balance accomplished by how much of heat the ocean can store in the summer to release it in the winter seasons and by how much it exchanges when it interacts with the atmosphere. Looking for another perspective, the amount of heat advected by the oceans corresponds to a barotropic and baroclinic transport which are geostrophic and an agestrophic Ekman component related to transport caused by the interaction of the ocean and the surface winds.

One of the main concern of the scientific community is to be able to collect evidences for climate change by analyzing long time–series of data or predict it by using ocean models. In both cases it is required a continuous time–series which in case of meridional heat flux is not available yet.

Changes in oceanic heat storage (HS) are associated with density changes in the water column and thus, with the sea surface height anomalies [*Gill and Niiler*, 1973]. It is important to estimate HS to improve our understanding of air–sea interactions and its contribution to climate change.

Estimates of HS are traditionally based on in situ measurements [*Wyrtki and Uhrich*, 1982; *Yan et al.*, 1995] or

[1]Instituto Nacional de Pesquisas Espaciais (INPE), São José dos Campos, São Paulo, Brazil
[2]Jet Propulsion Laboratory, California Institute of Technology, Pasadena, California

on climatological datasets [*Hsiung et al.*, 1989; *Moisan and Niiler*, 1997]. Most recently, HS has been estimated using altimetry data. *White and Tai* [1995] derived a linear relationship between the sea level anomaly measured by TOPEX/POSEIDON (T/P) and the HS estimated from XBT data and found correlations greater than 0.6 over the northern hemisphere. *Wang and Koblinsky* [1997] assumed simplifications on the buoyancy budget equation of the annual steric height variability to estimate the HS from T/P data and found a good agreement with XBT estimates over the North Atlantic. *Chambers et al.* [1997] showed that the mean heat storage rate (HSR) estimated from T/P agrees with those computed from monthly mean temperatures to within 30 Wm^{-2}. *Chambers et al.* [1998] found good agreement between T/P based HS estimates and those from the Tropical Ocean-Atmosphere (TAO) buoys.

The sea surface height anomalies are caused by dynamical and thermodynamical processes associated with various temporal and spatial scales. The objective of this study is to estimate the HS from T/P sea surface height anomalies and to identify those processes at four oceanographic sites where long time series of in situ data are available for validation. The comparison between in situ and satellite derived HS shows discrepancies that can be related to haline effects. These effects are relatively strong in coastal regions, decreasing toward the open ocean *Tabata et al.* [1986]. In this study, we demonstrate that a haline height correction significantly improves the satellite derived HS and that this correction should be based on in situ rather than climatological estimates.

Another component of the oceanic heat flux is represented by Ekman heat flux which can be obtained using satellite scatterometer data. Time–series of ocean temperature and wind stress data provide us a unique opportunity to observe seasonal and interannual variations in the heat observations.

In a global scale, the Ekman heat flux have been previously estimated using wind stress from in situ climatological data [*Kraus and Levitus*, 1986; *Levitus*, 1987; *Adamec et al.*, 1993] and from satellite–derived winds [*Ghirardelli et al.*, 1995]. Ekman heat flux is also estimated for specific locations when combined with direct measurements of the meridional heat flux [*Hall and Bryden*, 1982; *Bryden et al.*, 1991; *Macdonald and Wunsch*, 1996; *Sato and Rossby*, 2000]. *Ghirardelli et al.* [1995] investigated spatial and temporal variability of the Ekman heat flux using wind data from the Special Sensor Microwave Imager (SSMI) satellite data and sea surface temperature (SST) from Advanced Very High Resolution Radiometer (AVHRR) satellite data.

One of the main concerns when estimating the Ekman heat flux is the depth range of the ocean that should be considered to compensate the mass flux in the Ekman layer. As pointed out by *Montgomery* [1974] the heat flux should be estimated for system where the net mass flux is zero otherwise the heat flux is dependent on a arbitrarily defined reference temperature. *Böning and Herrmann* [1994] results from a high–resolution model of the Atlantic showed that the mass flux of the whole water column is necessary to compensate the surface Ekman mass transport.

The high spatial and temporal resolution and the directional information of the wind provided by the scatterometer satellite data can help to improve the estimates of the Ekman heat flux. The objective of this study is to investigate what is the relative importance of several bands of the frequency–zonal wavenumber of the wind–stress in establishing the variability of the Ekman heat flux using a 2D filtering method [*Polito et al.*, 2000].

The objetive of the paper is to illustrate two applications of the satellite data in estimating heat flux. To improve readability the paper will be split into two parts corresponding to each component: heat storage and Ekman heat flux.

Heat storage from altimeter

Method

The HS of an observed temperature profile is

$$HS = \rho C_p \int_{-h}^{0} T(z)dz, \tag{1}$$

where ρ is the density of seawater, C_p is the specific heat at constant pressure, $T(z)$ is the temperature profile, and h is the depth to which the temperature is integrated. HS is expressed in units of J m^{-2}.

The heat storage anomaly (HS′) is estimated from the filtered height anomaly (η) according to the linear relation *Chambers et al.* [1997]

$$HS' = \frac{\rho C_p}{\alpha}(\eta + \eta_h), \tag{2}$$

where α is the thermal expansion coefficient and η_h the height correction for the haline effect.

The product $\rho C_p(x, y, t)$, a function of longitude, latitude and time, is derived from climatological maps of the World Ocean Atlas 1994 (WOA94) *Levitus and Boyer* [1994] for a $1° \times 1°$ grid and is averaged from the surface to a depth h. $\alpha(x, y, t)$ is estimated by averaging from the surface to a depth h the climatological α profile weighted by layer thickness and temperature anomaly.

$\eta_h(x, y, t)$ is estimated by the integral of the product of the climatological haline contraction coefficient, β, and the salinity anomaly (residual after subtracting the annual mean) profiles from the surface to a depth h

$$\eta_h = \int_{-h}^{0} \beta \Delta S dz. \tag{3}$$

The original TOPEX/POSEIDON (T/P) sea surface height anomaly (η_o) is decomposed using 2D finite impulse response filters *Polito and Cornillon* [1997]; *Polito et al.* [2000]. This method uses previous knowledge of the spectral composition of the signal (approximate period and wavelength) to separate it into additive components:

$$\eta_o = \eta_t + \eta_w + \eta_r = \eta + \eta_r. \tag{4}$$

η_t is the basin–wide variability, mostly due to seasonality and advection. η_w is the meso to large–scale propagating signal composed mainly of baroclinic Rossby, Kelvin and instability waves. η_r is the small to meso–scale non–propagating eddy variability.

Data

The three selected sites are the sections from the California Cooperative Oceanic Fisheries Investigations (CalCOFI) cruises *Lynn and Simpson* [1987], the station ALOHA from the Hawaii Ocean Time series Program (HOT) *Karl and Lukas* [1996], and the station "S" in Bermuda (HyS) *Schroeder and Stommel* [1969] (Figure 1). Relatively long time series of temperature and salinity measurements are available concurrent with T/P data in these locations.

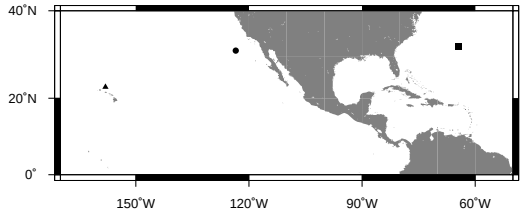

Figure 1. Location of the in situ data: triangle represents the HOT station, square the HyS, and circle the CalCOFI area.

The general procedure consists of linearly interpolating individual temperature and salinity profiles in the vertical. Stations with gaps larger than one standard depth were discarded. Missing surface data (above 25 m) were extrapolated by repeating the first measured value upward assuming that the data were within the mixed layer. Missing data in the deepest part of the profile (below the main thermocline) were extrapolated using the local mean gradient.

The integral in Equation 1 is calculated to a depth h below the main thermocline. For each time series the long–term mean is computed with the maximum number of complete years of data. The in situ HS′ is estimated by removing this mean. The T/P HS′ comes from Equation 2. To evaluate the role of η_h in determining the T/P HS′, three cases are studied: no salinity, climatological (WOA94), and in situ salinity.

Results

The decomposition of the altimeter signal as proposed in equation 4 allows us to examine the T/P signal at 32.5 °N in the Atlantic (Figure 2). The slanted patterns indicate propagation as highs and lows progress in space and time. Both η_{12} and η_6 increase in amplitude west of $\sim$ 30°W particularly during 1995 and 1996. Semiannual and annual waves cross the whole basin at a slightly higher phase speed on the western half of the basin compared to the eastern half.

The comparison of results is based on the root mean square (rms) difference and correlation between the in situ and T/P HS′ for the three sites (Table 1).

The portion of the HyS time series used in this study spans from 1993 to 1997 (Figure 3) and has on average one measurement every 15 days. The HS′ time series from both sources were interpolated to one month resolution. The T/P HS′ are in better agreement (lower rms difference and higher correlation) with in situ HS′ when the haline correction is based on in situ rather than climatological salinity. When

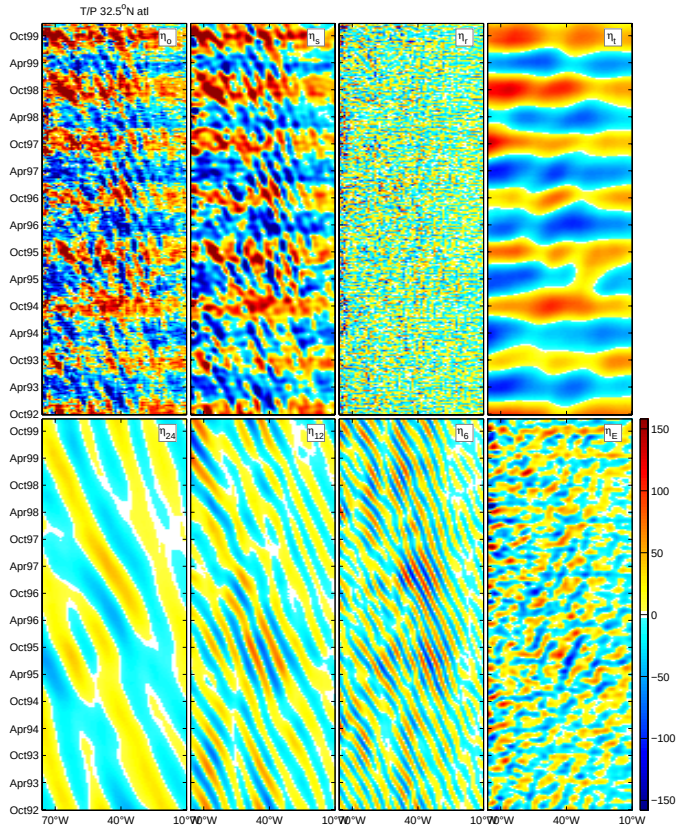

Figure 2. Sea surface height anomaly components (in mm) from T/P as a function of longitude and time at 32.5°N (HyS) in the Atlantic.

Table 1. Rms difference (in $10^7 J\,m^{-2}$) and correlation between in situ and T/P derived HS′ with (climatological/in situ) or without haline correction.

Source	No sal.		WOA94		in situ	
	rms	corr.	rms	corr.	rms	corr.
HyS	71	.77	69	.76	64	.86
HOT	65	.63	73	.57	56	.75
CalCOFI	67	.49	68	.49	56	.67

the salinity is not used, the rms difference and correlation are about the same as when the climatological salinity is used.

Results at HyS are in better agreement after 1995 as the dominant signal in the heat storage spectrum shifts from semiannual to annual *Polito et al.* [2000]. Lower rms difference and higher correlation (52×10^7 J m^{-2} and 0.90) are obtained for the 1995–97 period compared to 1993–95 (75×10^7 J m^{-2} and 0.80). As HyS nearly coincides with a T/P cross-over latitude the zonal spacing between samples is maximum. This distance is approximately twice the wavelength of the local semiannual Rossby waves. Therefore, T/P cannot properly resolve the early semiannual signal which results in spatial aliasing *Parke et al.* [1998] and degradation of the correlation.

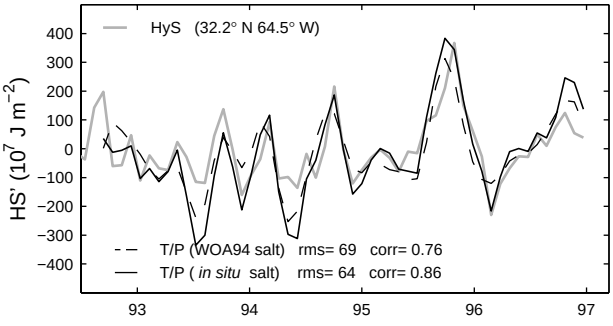

Figure 3. Comparison of the HS′ between HyS (gray) and T/P with climatological (dashed) and in situ (solid) haline correction.

The time series used at HOT spans from 1993 to 1998, and has a sampling period of 40 days (Figure 4). Both time series were interpolated to monthly resolution for comparison. Similarly to the previous case, the results when including in situ salinity are significantly better than using the climatology. In fact, when the salinity is not used, the rms and the correlation are better than using climatology.

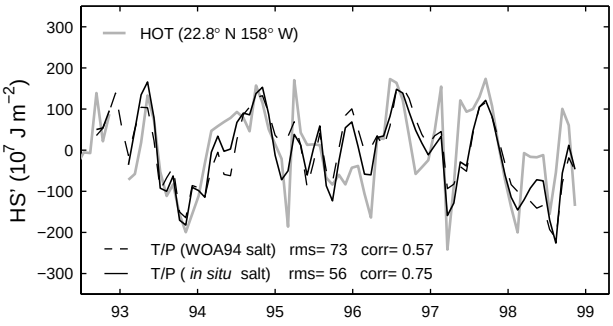

Figure 4. Same as Figure 3 but at HOT.

The CalCOFI cruises are composed of an array of stations near the California coast and the used time series coincides with T/P between 1993 and 1998. Satellite measurements of the sea surface height degrade near the coast due, to a large extent, to local tides that are inadequately modeled in the T/P data and spread westward by the filter. Thus, correlations decrease and rms differences increase toward the coast. A strong gradient in both rms and correlation is located in the approximate SE–NW diagonal of Figure 6. Therefore, only eleven stations west of this gradient were considered. Station 90/110 located at 30.75°N, 123.33°W gave results which were decorrelated with all stations in its vicinity and was excluded from the analysis. The CalCOFI stations have lower temporal resolution compared to the other sites, with one sample every 90 days. The T/P time series was interpolated to this resolution.

In general, away from the influence of the coast the results favor the use of in situ salinity. As shown in the two stations in Figure 5 the T/P estimates including salinity effects from in situ measurements improved significantly. As observed for other regions the inclusion of a climatological salinity is detrimental to the results.

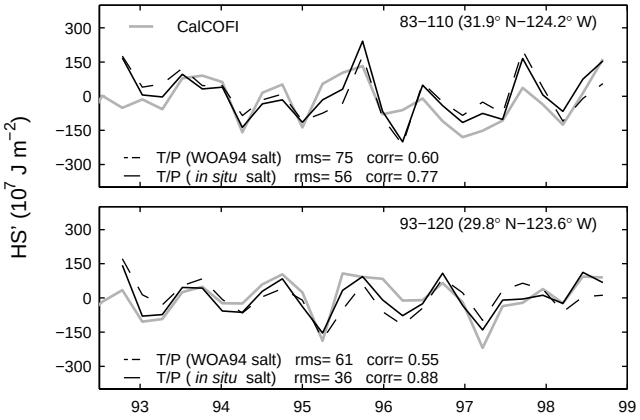

Figure 5. Same as Figure 3 but at CalCOFI.

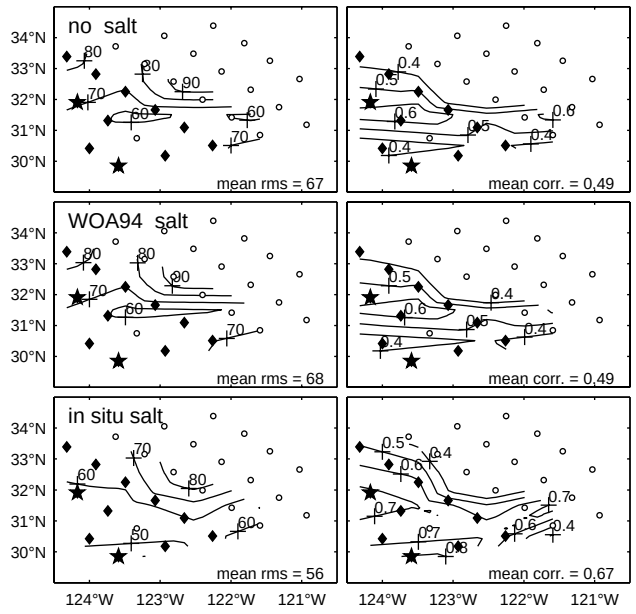

Figure 6. Rms difference (left) and correlation coefficient between CalCOFI and T/P estimates of HS′ in $10^7 J\,m^{-2}$. Diamonds (circles) mark the stations used (discarded). Stars indicate the stations used in Figure 5.

Conclusions

Time series of temperature and salinity measurements from three hydrographic sites were used to evaluate the importance of haline effects in the determination of the heat storage anomaly from sea surface height anomaly. In all locations (HyS, HOT, and CalCOFI) the haline effects were estimated for three cases: absent, climatological (WOA94), and in situ salinity profiles. The results based on climatological salinities are equal or worse than not including haline effects at all. The use of in situ salinity estimates significantly augmented the correlations and decreased the rms differences in the HS′ estimates.

At HyS the rms difference decreased by 5×10^7 J m^{-2} and the correlation increased by 0.1 when using in situ instead of climatological salinity. Better results were obtained from the other sites. At HOT, the rms decreased by 17×10^7 J m^{-2}

and the correlation improved by 0.18 while at CalCOFI, the average rms decreased by 12 $\times$ 10^7 J m^{-2} and correlations increased by 0.18. These results stress the importance of salinity measurements concurrent with satellite altimeter measurements to study sub–surface processes. Although in situ salinity measurements are sparse the lack of a relatively small haline correction does not preclude the use of altimeter data for oceanic heat storage estimation.

Meridional Ekman heat flux

Method and data

The meridional Ekman heat flux is defined as:

$$E = -c_p \int_0^L \frac{\tau_x}{f}(\theta_e - \bar{\theta})\, dx. \tag{5}$$

where c_p is the specific heat at constant pressure which is assumed to be 4100 $J\,kg^{-1}\,K^{-1}$; τ_x is the zonal component of the wind stress; f is the Coriolis parameter; θ_e is the potential temperature of the Ekman layer and $\bar{\theta}$ is the mean potential temperature of the water column.

Previous studies implicitly assumed that the depth of the Ekman layer is much smaller than the mixed layer depth. Therefore, the SST was used as the first approximation of the temperature of the Ekman layer [*Kraus and Levitus*, 1986; *Levitus*, 1987; *Adamec et al.*, 1993; *Ghirardelli et al.*, 1995]. In this study the mean temperature within the Ekman layer (θ_e) was obtained from a weighted average using the meridional velocities profiles as weights. The meridional Ekman velocity profile $v(z)$ is given by *Kundu* [1990]:

$$v(z) = \frac{-\tau_x/\rho}{\sqrt{f\nu}} e^{\frac{z}{\delta}} \sin(\frac{-z}{\delta} + \frac{\pi}{4}), \tag{6}$$

where ρ is the seawater density, ν is the eddy viscosity coefficient, and δ is the depth of the Ekman layer. As $v(z)$ will be used as weights, only the functional form v_n is relevant to this problem:

$$v_n(z) = e^{\frac{z}{\delta}} \sin(\frac{-z}{\delta} + \frac{\pi}{4}). \tag{7}$$

The depth of the Ekman layer is assumed to be constant and δ = -100 m. The velocity weights are estimated for the standard depths of z = 0, -10, -20, -30, -50, -75, -100 m and normalized to make the sum of the weights equal to one. The seven coefficients are: $v_n(0) = 0.2263$, $v_n(-10) = 0.2184$, $v_n(-20) = 0.1988$, $v_n(-30) = 0.1726$, $v_n(-50) = 0.1150$, $v_n(-75) = 0.0539$ and $v_n(-100) = 0.0151$.

At each location the mean velocity–weighted potential temperature ($\theta(x, y)$) is obtained from:

$$\theta_e(x, y) = \sum_{z=0}^{-100} v_n(z)\theta(x, y, z) \tag{8}$$

The temperature profiles in the Ekman layer are composed by a combination of SST from the Reynolds data set from 1993 to 1998 and monthly mean climatological temperatures from 10 to 100 m from the World Ocean Atlas 1998, Figure 7. The SST data used in this study are interpolated to a 1° $\times$ 1° $\times$ 10 days resolution grid. The sub–surface profiles are built from the monthly means.

The Ekman layer volume transport should be balance by an equal and in opposite direction compensating flow in the deep ocean so that the mass conservation condition is satisfied at each latitude. According to *Böning and Herrmann* [1994] the return flow should extend to at least 3000 m in the extra-tropical region. $\bar{\theta}$ is the average temperature of the volume transported by the ocean necessary to compensate the Ekman volume flux. Since temperature profiles for the whole ocean depth are not available the monthly climatological means of $\bar{\theta}$ from the World Ocean Atlas 1994 [*Levitus and Boyer*, 1994] which contains profiles from 0 to 5500 m are used, Figure 7.

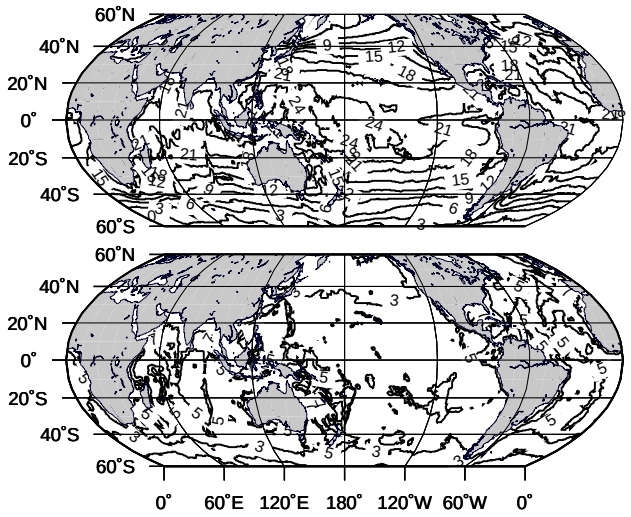

Figure 7. Ekman temperature annual mean average (top) and the ocean mean temperature (bottom).

The mean temperature of the ocean is very similar to the values used by previous studies. However, the use of an Ekman temperature which is generally smaller than the SST leads to a smaller Ekman heat flux. This matter will be discussed later.

The wind data are obtained from the European Research Satellite 1 and 2 (ERS-1/2). The zonal component of the wind stress (τ_x) is calculated based on standard procedure following the *Large and Pond* [1981] formulation. τ_x is interpolate to match the same resolution in space and time as the SST data set.

Filtering the wind stress Temporal changes in the meridional Ekman heat flux are affected by changes in both the wind stress and temperature fields. Here we investigate the relative contribution of some of the components of τ_x to the Ekman heat flux. The effect of the temperature is not considered in this study. First, because we lack higher resolution temperature profiles since only the SST is measured and the rest of the profile is climatological. Second, it seems that most of the variability observed from the Ekman heat flux is dominated from the variances of the wind stress field. A further study using a model output temperature profiles

should be conducted to investigate the role of the temperature in the variability of the Ekman heat flux.

The ERS-1/2 zonal component of the wind stress anomaly is decomposed using a 2D finite impulse response filtering [*Polito et al.*, 2000] as:

$$\tau_x = \bar{\tau} + \tau_l + \tau_w + \tau_m + \tau_s. \quad (9)$$

$\bar{\tau}$ is the long–term mean component. τ_l is the large basin–wide non–propagating variability, mostly due to seasonal changes. τ_w is composed mainly of signals related to oceanic first–mode baroclinic Rossby waves. τ_m includes a variety of meso–scale eddy variability. τ_s are the small–scale, non–propagating signals.

Results

The mean meridional Ekman heat flux estimated using scatterometer satellite data as a function of latitude is poleward between the tropics for the Atlantic and Pacific and in the tropical South Indian Ocean. An equatorial band from 4°S to 4°N is excluded from the study region, Figure 8.

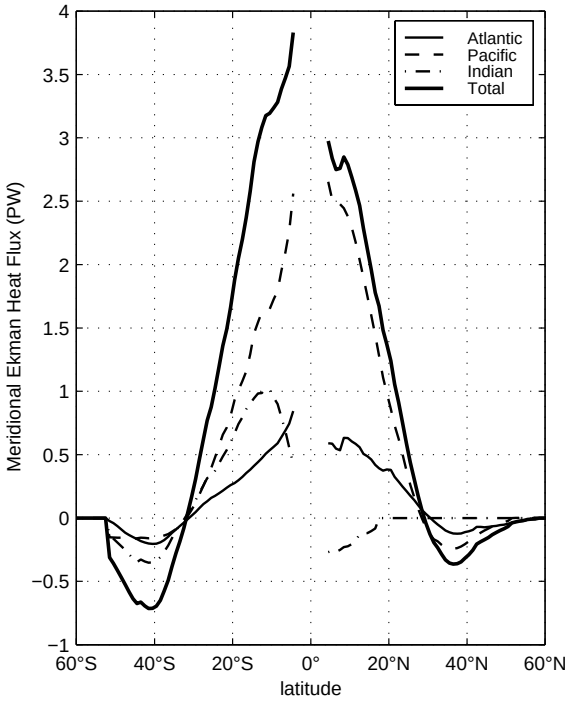

Figure 8. Mean Ekman heat flux (PW) for all ocean basins. Positive values represent poleward flux.

There are some significant differences in the annual mean and cycle of the Ekman heat flux when compared to previous studies. The magnitude of the zonally averaged annual mean of the poleward Ekman heat flux estimated by this study is much lower than the ones determined using climatological data [*Levitus*, 1987]. However, it is only slightly lower when compared to *Ghirardelli et al.* [1995] using SSMI winds. The source for the large differences compared to the climatology is the wind data. Scatterometer data have higher spatial and temporal resolution and tend to capture the high frequency variability while the climatological fields are more much smoother. In comparison with the estimates based on SSMI satellite winds in which they have similar resolution the source of the differences is the definition of the temperature in the Ekman layer.

A significant part of the difference between our results and previous studies can be attributed to the choice of the definition of the temperature of the Ekman layer. In the previous studies the Ekman temperature is approximated by the SST. In this study we used the velocity weighted temperature. For comparison the Ekman heat flux is estimated using sea surface and the velocity weighted temperatures, Figure 9. The zonally average annual mean when using SST is slightly higher and looks much more like the results presented by *Ghirardelli et al.* [1995].

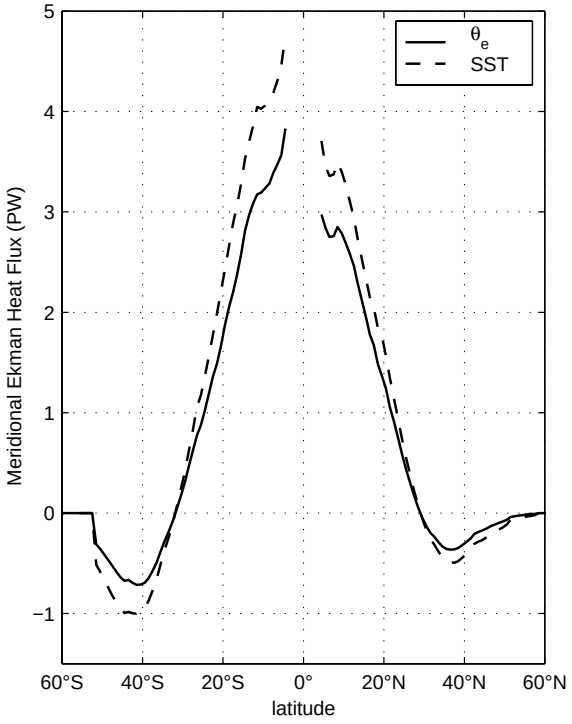

Figure 9. The Ekman heat flux of the World Ocean as a function of latitude using the temperature of the Ekman layer or SST.

The amplitude of the annual cycle is similar for the Atlantic and the Pacific but the patterns are asymmetric between the northern and southern hemispheres, Figure 10. For latitudes lower than 30° the heat transported by the Ekman layer is poleward in the Atlantic and Pacific except for a equatorward flux near 5°N during the fall months. These areas of weak equatorward Ekman flux are caused by a change in the wind pattern because of the displacement of the ITCZs [*Levitus*, 1987]. For latitudes higher than 30° the Ekman flux is mostly equatorward in all oceans. In the North Indian Ocean there is a strong equatorward Ekman heat flux from April to November consistent with the wind regime characteristic of the summer Moonson. *Levitus* [1987] pointed out that this signal dominates the global zonally averaged Ekman heat transport. However, small contributions from the Atlantic and Pacific are detected using a more highly resolved data such as the winds from the scatterometer.

The temporal and spatial variability of the total Ekman

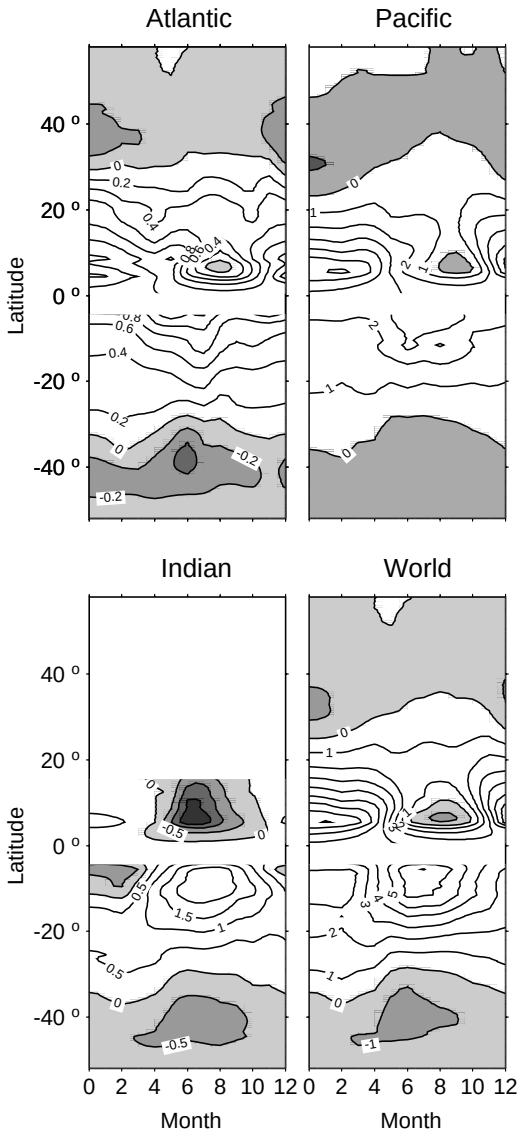

Figure 10. Annual cycle of zonally integrated meridional Ekman heat flux. Shaded regions represent equatorward heat flux.

heat flux is examined by decomposing the wind stress signal in several frequency band components using equation 9. The strongest point of this filtering method is its capability of decomposing different components of propagating and non–propagating features in a time–space field without interfering with the final results. Longitude–time diagrams can be constructed at specific latitude lines to analyze the progression of each frequency band. For illustration, a x–t diagram is shown for the Ekman heat flux anomaly (total minus an annual mean) for the latitude of 40°S in the Atlantic, Figure 11. For present study, only the variability in the wind stress is accounted for, disregarding the changes due to variability in the temperature in the Ekman layer.

The six panels on Figure 11 represent the contribution from the main components in the total Ekman heat flux signal. The first panel is the total anomaly before the filtering. The second panel on the top shows Ekman heat anomaly using the wind stress component $\bar{\tau}$, the long–term mean com-

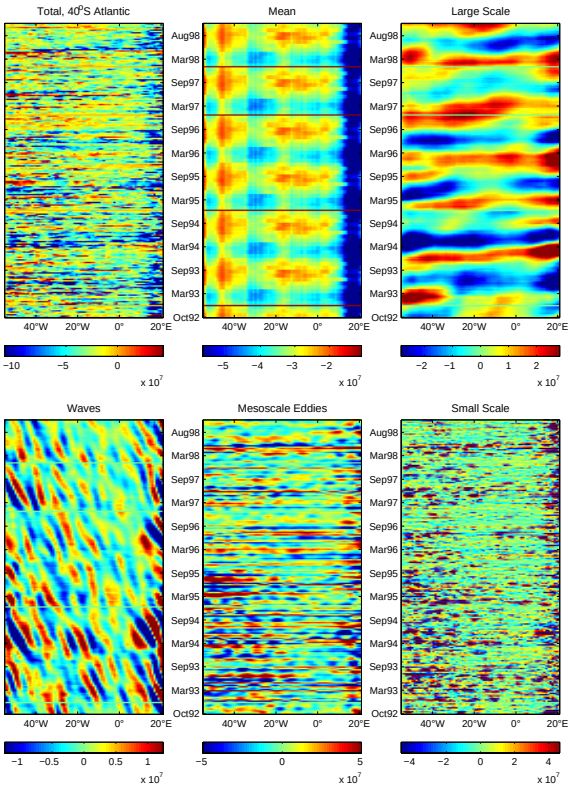

Figure 11. Longitude–time diagrams of τ_x at 40 °S in the Atlantic for the original signal and each one of the components.

ponent. Since the contribution from this wind stress component is a constant then the variations in the heat flux represent the seasonal changes due to variability in the temperature field. This is the only place that the temperature variability can be accounted for. The large scale features in the last top panel are mostly due to the changes in the non–propagating signal in the wind stress anomaly associated with seasonal cycle. The three panels in the bottom are related to propagating signals present in the wind stress anomaly. The first one is dominated by the oceanic first–mode baroclinic Rossby waves, while the other two include a variety of meso–scale and small-scale eddy variability respectively. At 40°S in the Atlantic Ocean the largest variability in the Ekman heat flux comes from the meso– and small–scale components. That is, the variance in the total heat anomaly signal associated with the wind stress is caused by changes at these scale of propagating features.

Diagrams such as in Figure 11 can be made at each latitude for a more detailed study. For this study the variability of each component is investigate for a long–term averaged scale for each oceanic basin to concentrate more in the spatial patterns. The relative contribution of each of the spectral components in the Ekman heat flux is calculated to identify which are the dominant source of variability for each ocean basin, Figures 12, 13, and 14.

The meridional distribution of the % variance of the spectral components in the Atlantic can be described generally as composed by two regimes limited at about 15° latitude, Figure 12. Poleward of 15° the variance in the total Ekman heat

is dominated by the meso– and small–scale components while equatorward is more dominated by the mean and large–scale components. As noted earlier for the patterns in the annual mean amplitude the meridional distribution of the variance is not symmetric either. The northern hemisphere is marked by the dominance of the meso–scale variability while in the southern hemisphere the meso–scale variability are equally important as the small–scale ones. Large–scale variability due to the wind stress is more important just north of the Equator while the at the south the temperature changes dictate the Ekman heat flux variability. The contribution from the wave components is small throughout the basin.

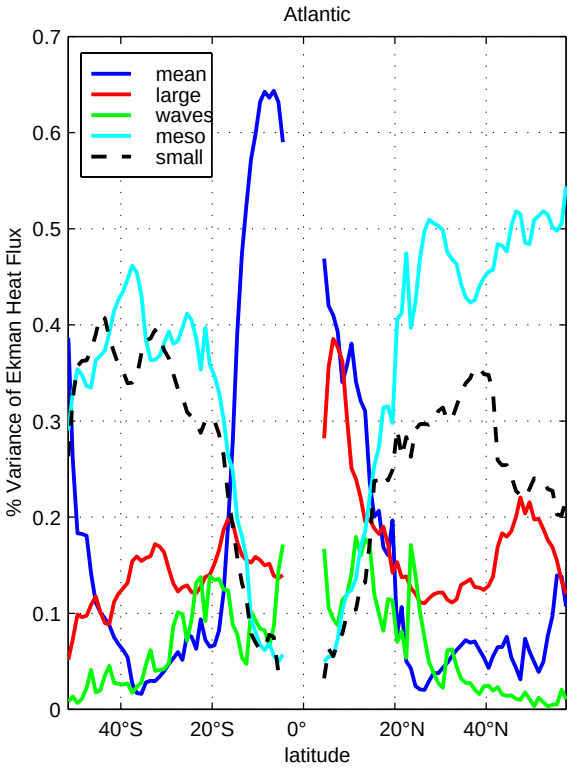

Figure 12. Zonal temporal mean of the % Variance of the spectral components of the Ekman heat flux in the Atlantic Ocean.

The Pacific Ocean shows a similar two–regime meridional distribution of the spectral components. However, the contribution of the mean signal is not as important as in the Atlantic in the equatorial region. The relative importance of the Rossby waves increase in the Pacific where the wave contribution is comparable to the mean and large-scale components near the Equator.

At the Southern Indian Ocean two regimes are separated at about 20°S. Equatorward of this latitude the large–scale and the waves components seems to dominate the heat variability while poleward the the processes are more dominated by a competing effects of changes in meso– and small–scale level. South of 50 °S, similar to the Atlantic, changes in the long–term mean becomes the most important contribution. The Northern Indian Ocean is dominated by the large–scale variability consonant with seasonal changes in the wind patterns associated with the summer monsoon.

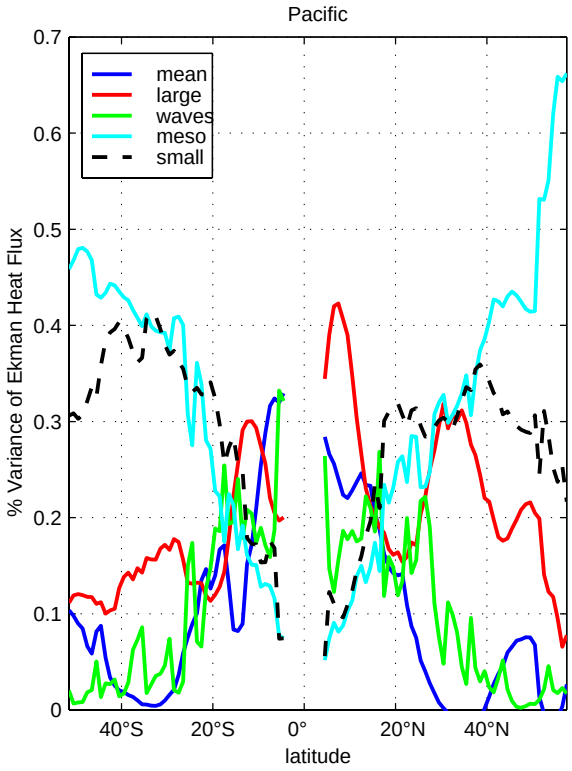

Figure 13. Zonal temporal mean of the % Variance of the spectral components of the Ekman heat flux in the Pacific Ocean.

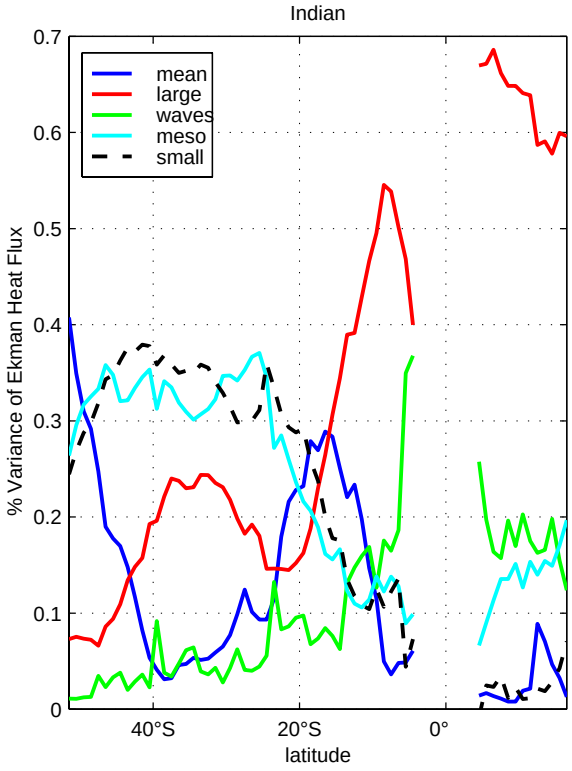

Figure 14. Zonal temporal mean of the % Variance of the spectral components of the Ekman heat flux in the Indian Ocean.

Conclusions

The Ekman heat flux is examined using a new set of satellite measurements of wind provided by the scatterometers. Compared to previous studies the present approach is based on a more strict definition of temperature of the Ekman layer. Here the temperature shows a velocity averaged effects as opposed to just taking the temperature at the surface. By definition the heat flux requires to be estimated in a mass conservative system. To accomplished that the whole ocean layer has to be accounted to compensate this warm, superficial, and fast–flowing Ekman layer [*Böning and Herrmann*, 1994]. The difference in temperature between these two layers is the major source of discrepancies between this and *Ghirardelli et al.* [1995] studies who also used satellite derived from but from SSMI data.

The zonal mean Ekman heat flux estimates from this study is much lower compared to climatology [*Levitus*, 1987] because a combination of factors such as the difference in definition of the Ekman temperature and the more reliable wind stress measurements. The general pattern in the zonal mean is very similar in the various studies in which the heat is transported poleward between the tropics and equatorward at higher latitudes for most of the oceans. The exception is the Northern Indian Ocean where due to the monsoon wind regime the transport is equatorward.

The contribution of several frequency bands in the zonal component of the wind stress data is analyzed to examine their relative importance in the total Ekman heat flux variability. In general, between the latitudes of 15° the variance of the Ekman heat flux is dominated by the large–scale variability of the wind stress and temperature fields. Poleward of 15° the meso– and small–scale variability of the wind stress explain most of the variance in the heat flux.

Acknowledgments. This study was performed at the Jet Propulsion Laboratory, California Institute of Technology, under contract with the National Aeronautics and Space Administration (NASA). The study is jointly supported by the Physical Oceanography and Earth Observing System Interdisciplinary Sciences Programs of NASA.

References

Adamec, D., M. M. Rienecker, and J. M. Vukovich, The time–varying characteristics of the meridional Ekman heat transport for the world ocean, *J. Phys. Oceanogr.*, *23*, 2704–2716, 1993.

Böning, and P. Herrmann, Annual cycle of poleward heat transport in the ocean: results from high resolution modeling of the North and Equatorial atlantic, *J. Phys. Oceanogr.*, *24*, 91–107, 1994.

Bryden, H. L., D. H. Roemmich, and J. A. Church, Ocean heat transport across 24°N in the Pacific, *Deep-Sea Res.*, *40*, 297–324, 1991.

Chambers, D. P., B. D. Tapley, and R. H. Stewart, Long–period ocean heat storage rates and basin–scale heat fluxes from TOPEX, *J. Geophys. Res.*, *102(C5)*, 10,525–10,533, 1997.

Chambers, D. P., B. D. Tapley, and R. H. Stewart, Measuring heat storage changes in the equatorial Pacific: A comparison between TOPEX altimetry and tropical atmosphere–ocean buoys, *J. Geophys. Res.*, *103(C9)*, 18,591–18,597, 1998.

Ghirardelli, J. E., M. M. Rienecker, and D. Adamec, Meridional Ekman heat transport: estimates from satellite data, *J. Phys. Oceanogr.*, *25*, 2741–2755, 1995.

Gill, A. E., and P. P. Niiler, The theory of the seasonal variability in the ocean, *Deep-Sea Res.*, *20*, 141–177, 1973.

Hall, M. M., and H. L. Bryden, Direct estimates and mechanisms of ocean heat transport, *Deep-Sea Res.*, *29*, 339–359, 1982.

Hsiung, J., R. E. Newell, and T. Houghtby, The annual cycle of oceanic heat storage and oceanic meridional heat transport, *Q. J. Roy. Meteor. Soc.*, *115*, 1–28, 1989.

Karl, D. M., and R. Lukas, The Hawaii Ocean Time-series (HOT) Program: Background, rationale and field implementation, *Deep Sea Research II*, *43*, 129–156, 1996.

Kraus, E. B., and S. Levitus, Annual heat flux variations across the tropic circles, *J. Phys. Oceanogr.*, *16*, 1479–1486, 1986.

Kundu, P. K., *Fluid Mechanics*, Academic Press, 1990, 638 pp.

Large, W. G., and S. Pond, Open ocean momentum flux measurements in moderate to strong winds, *J. Phys. Oceanogr.*, *11*, 324–336, 1981.

Levitus, S., Meridional Ekman heat fluxes for the world ocean and individual ocean basins, *J. Phys. Oceanogr.*, *17*, 1484–1492, 1987.

Levitus, S., and T. P. Boyer, World Ocean Atlas 1994, *Tech. Rep. Vol. 4: Temperature*, National Oceanographic Data Center, Ocean Climate Laboratory, 1994, 129 pp.

Lynn, R. J., and J. J. Simpson, The California current system: The seasonal variability of its physical characteristics, *J. Geophys. Res.*, *92(C12)*, 12,947–12,966, 1987.

Macdonald, A. M., and C. Wunsch, A global estimate of the ocean circulation and heat fluxes, *Nature*, *382*, 436–439, 1996.

Moisan, J. R., and P. P. Niiler, The seasonal heat budget of the North Pacific: Net heat flux and Heat Storage rates (1950–1990), *J. Phys. Oceanogr.*, *28*, 401–421, 1997.

Montgomery, R. B., Comments on "Seasonal variability of the Florida current," by Niiler and Richardson, *J. Mar. Res.*, *32*, 533–535, 1974.

Parke, M. E., R. L. G. Born, C. McLaughlin, and C. Tierney, Altimeter sampling characteristics using a single satellite, *J. Geophys. Res.*, *103*, 10,513–10,526, 1998.

Polito, P. S., and P. Cornillon, Long baroclinic rossby waves detected by TOPEX/POSEIDON, *J. Geophys. Res.*, *102*, 3215–3235, 1997.

Polito, P. S., O. Sato, and W. T. Liu, Characterization of the heat storage variability from TOPEX/POSEIDON at four oceanographic sites, *J. Geophys. Res.*, *105(C7)*, 16,911–16,921, 2000.

Sato, O. T., and T. Rossby, Seasonal and low frequency variability in the meridional heat flux at 36°N in the North Atlantic, *J. Phys. Oceanogr.*, *30(3)*, 606–621, 2000.

Schroeder, E., and H. Stommel, How representative is the series of Panulirus stations of monthly mean conditions off Bermuda?, *Prog. Oceanogr.*, *5*, 31–40, 1969.

Tabata, S., B. Thomas, and D. Ramsden, Annual and interannual variability of steric sea level along line p in the northeast pacific ocean, *J. Phys. Oceanogr.*, *16*, 1378–1398, 1986.

Wang, L., and C. Koblinsky, Can the Topex/Poseidon altimetry data be used to estimate air–sea heat flux in the North Atlantic?, *Geophysical Research Letters*, *24(2)*, 139–142, 1997.

White, W. B., and C. K. Tai, Inferring interannual changes in global upper ocean heat storage from TOPEX altimetry, *J. Geophys. Res.*, *100*, 24,943–24,954, 1995.

Wyrtki, K., and L. Uhrich, On the accuracy of heat storage computations, *J. Phys. Oceanogr.*, *12*, 1411–1416, 1982.

Yan, X. H., P. P. Niiler, S. K. Nadiga, R. H. Stewart, and D. R. Cayan, Seasonal heat storage in the North Pacific: 1976–1989, *J. Geophys. Res.*, *100(C4)*, 6899–6926, 1995.

O. T. Sato, P. S. Polito, Instituto Nacional de Pesquisas Espaciais (INPE), Divisao de Sensoriamento Remoto, Av.

dos Astronautas, 1758, Jd. da Granja, Sao Jose dos Campos, SP 12227-010, Brazil, (e-mail: olga@ltid.inpe.br; polito@ltid.inpe.br

W. Timothy Liu, Jet Propulsion Laboratory, California Institute of Technology, 4800 Oak Grove Dr., MS 300-323, Pasadena CA 91109, (e-mail: liu@pacific.jpl.nasa.gov)